Astron. Astrophys. 280, 365–372 (1993)

ASTRONOMY AND ASTROPHYSICS

Hα survey of the Small Magellanic Cloud*

Etienne le Coarer[1], Margarita Rosado[2], Yvon Georgelin[3], Annick Viale[3], and Guillermo Goldes[4]

[1] Observatoire de Grenoble BP53X Grenoble CEDEX
[2] Universidad Nacional Autonoma de Mexico, Instituto Astronomia. Apartado Postal 70-264, Ciudad Universitaria, CP-04510 Mexico,D.F.
[3] Observatoire de Marseille 2, pl Le Verrier F-13248 Marseille France
[4] Observatorio Astronomico, Laprida 854, 5000 Cordoba, Argentina

Received April 14, accepted June 24, 1993

Abstract. We present the first results of a kinematical Hα survey of the Small Magellanic Cloud. We discuss the specialized instrumentation used in this survey (telescope, focal reducer, scanning Fabry-Perot interferometers and photon counting system). We discuss also the main aspects of the data reduction. We compare the quality of our data with those obtained by other authors. We present images of the SMC showing both the intensity and the radial velocity of the HII regions and a catalogue of velocities and Hα fluxes of 143 HII regions in this galaxy. We find that the HII region distribution follows that of the HI and we verify the existence of a gradient in velocities along the bar.

Key words: galaxies: Magellanic Clouds – galaxies: kinematics – galaxies: ISM – HII regions

1. Introduction

The Small Magellanic Cloud (SMC) and the Large Magellanic Cloud (LMC) are the nearest external galaxies. Their position in a region of the sky of low reddening, their large apparent diameters, and the fact that both clouds are galaxies which have different properties (mass, rotation, chemical abundances, Hubble type, etc.) compared with our Galaxy, makes them very attractive for the study of objects of a given specific class such as HII regions, supernova remnants (SNRs), planetary nebulæ (PNe), wind bubbles and superbubbles. On the other hand, the SMC reveals a complicated structure. Studies of HI, yellow stars, PNe and diffuse ionized hydrogen reveal that several velocity components are present along the line of sight covering extended regions of the SMC. This complicated structure is probably due to an interaction of the SMC with the LMC or to a close encounter with our own Galaxy some 2 10^8 yr ago (Murai & Fujimoto 1980). The complicated kinematic structure of HI makes it difficult to establish a rotational pattern for the SMC and consequently, to have a clear understanding of the properties of this galaxy; this circumstance makes uncertain the derivation of the mass of the SMC from its rotation curve. Furthermore, it is important to know the depth of the SMC, for if the SMC has a large depth (Mathewson & Ford 1983; Martin et al. 1989), the prospect of studying a class of objects in the SMC at the same distance is no longer viable.

We have studied several bubbles, HII regions and SNRs in the LMC by means of a scanning FP interferometer (Laval et al. 1989 and 1992 and Rosado et al. 1990 and 1993). This allowed us to know the kinematics of these objects with a large angular resolution (2.6″/px) but with a modest angular field of view (8′). However, the limited field of view makes it difficult to carry out a photometric calibration of our observations because, in order to calibrate properly the Hα flux of a given region, it is necessary to observe, in the same field, another region already calibrated.

Simultaneously to the study of the ionized hydrogen structure of the SMC we wish to study specific classes of objects in the Magellanic Clouds, such as SNRs, wind bubbles, HII regions, superbubbles and PNe, to compare their properties with those of the objects of the same class located in other galaxies (in particular in the Milky Way) and to study the interaction of these objects with the parent galaxy and be able to understand the energy exchanges between stars and gas in a galaxy. Thus, we require a whole set of homogeneous observations with both high sensitivity and good coverage of important regions. In addition, we wish to discriminate between the kinematical components of a specific object and those of extended galactic sources (such as those detected both in the SMC and in the LMC; Songaila et al. 1985; Meaburn et al. 1984 and Rosado et al. 1990). These observations will also allow the study of the kinematics of the diffuse hydrogen which permeates the SMC. These reasons motivated us to undertake a survey of the SMC with equipment which ensures high sensitivity for the detection of monochromatic Hα emission, a large field of view and a spectral resolution comparable with that employed in our previous studies. In order to accomplish this we have used a small diameter telescope equipped with a focal reducer, a scanning FP

* Table 1 is only avaible in electronic form: see the editorial in A&A 1992, Vol. 266 N2, page E1

interferometer and a photon counting camera. With this equipment we have covered the whole Hα emission of the SMC and some selected regions of the LMC. The purpose of this paper is to report our first results derived from the observations of the SMC. In Sect. 2 we will describe the equipment used, the observations and the data reductions; in Sect. 3 we will determine the limiting sensitivity of our survey and discuss the problem of the spurious night sky emission lines ; in Sect. 4 we will discuss on the photometric calibration; in Sect. 5 we will present maps of the Hα emission of the SMC, built from several individual fields and presented in a mosaic, we will discuss the detection of H^+ loops which are closely related to IRAS filaments and, finally, we will present the determinations of radial velocities and Hα fluxes of 143 emission regions of the catalogue of Davies et al. (1976; herafter called DEM). In Sect. 6 we compare the results of this work with previous data. A preliminary discussion of the data is given in Sect. 7.

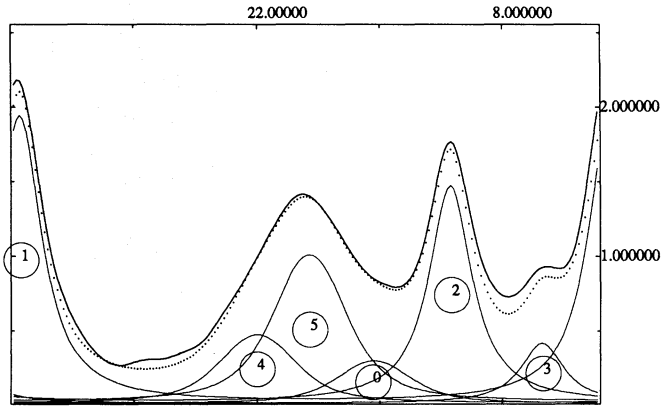

Fig. 1. Example of decomposition of profile seen in an "empty" field. Profiles 1,2 and 3 are nightsky emission lines and 4,0 and 5 are broad components L at 155kms^{-1}, VH at 195 kms^{-1} and H at 176 kms^{-1} with 5 and 10 erg cm^{-6}pc intensity. Coordinates are: number of counts and radial velocity channels

2. Description of the instrument

Descriptions and details of the equipment used in this survey can be found in Amram et al. (1991), le Coarer et al. (1992 and 1993). Here we give only some general aspects of the instrument. It is a dedicated 36 cm telescope equipped with a focal reducer, two scanning Fabry-Perot (FP) interferometers, a series of interference filters and a photon counting camera. Table 1 in Amram et al. (1991) and Le Coarer et al. (1992), gives the general characteristics of this equipment. We obtain FP data cubes which have an angular resolution of 9" (equivalent to 2.8 pc at the SMC distance of 65 kpc), a field of view of 38′ (covered by the 256 × 256 pixels of the photon counting camera) and the sampling spectral resolutions of 5 and 16 kms^{-1} at Hα, depending on the scanning FP interferometer used. Here we report only the results of our observations at a sampling spectral resolution of 16 kms^{-1}. The observational technique and the amount and types of data we obtain with this system is the same as that already described in Amram et al. (1991) and Le Coarer et al. (1992) ; we use here the same terminology. The data reduction is performed with dedicated software. The calibration of the 24 nebular interferograms is performed by scanning the diffuse light of both neon and hydrogen lamps. These calibration interferograms allow the derivation of the phase-map which gives the wavelength origin of each pixel. The instrumental profile is derived from the calibration interferograms obtained for the narrow line at lambda 659.895 nm of the Ne lamp. The profiles obtained for the Hα calibrations are broader because of the fine structure present for Hα and the low atomic weight of hydrogen (Meaburn 1970; Dyson & Meaburn 1971). The instrumental profile fits the classical Airy function characteristic of the instrumental response of the FP interferometer used in these observations. For each filter used, flat-field correction is performed using the addition of the calibration interferograms at Hα or those of a diffuse continuum source.

3. Night-sky parasitic lines and limiting emission measure

An Hα filter (λ_c = 656.9nm; $\delta\lambda$=1nm), shifted to the SMC redshift, is more or less transparent to the series of night-sky emission lines which ultimately set the limit of detection of the nebular emission. Within this range we detect, in order of importance, geocoronal Hα at 656.278nm, an OH nightglow lines at 656.872nm and 657.725nm.

Figure 1 shows a typical profile obtained from our radial velocity data on a window of 10 × 10 px in one of the fields; the window is located in a region where not much nebulosity is seen to identify the night-sky lines ; however, a faint nebular line is seen between the night-sky lines. As we can see, the radial velocities of the SMC nebulæ are well located relative to the positions of the night-sky lines for this particular FP interferometer. This implies that, in general, night-sky lines are easily discriminated against and subtracted from the interferograms for most of the velocity range of the SMC nebulosities. Extreme velocity nebulæ are less easy to discriminate against but, the fact that we can build a pattern of the night-sky emission over the whole field is an important help in the subtraction of the night-sky lines for these nebulæ. Thus, in conclusion, we can detect easily most of the nebular emission even if it has intensities below the night sky value. Nebular emission at extreme velocities can be studied only if its intensity is comparable with that of the night-sky lines. One of the results of this work is the improvement of the determination of the limiting Hα surface brightness quoted in Amram et al. (1991) and Le Coarer et al. (1992). Indeed, under the assumption that the limiting surface brightness corresponds to that of the OH 657.7nm line, we obtain, from three independent methods, a value for the limiting Hα surface brightness is:

$S(H\alpha)_{\rm lim} = (1.1 \pm 0.3)10^{-6}$erg cm^{-2}s^{-1}sr^{-1}

corresponding to a limiting emission measure

$EM_{\rm lim} = (11.3 \pm 2.6)$cm^{-6}pc

(for a T=10^4 K, Case B photoionized nebula), reached in an exposure time of 8280 s, which confirms our previous estimate. As stated before, this is a limit in the emission measure for radial velocity determination. The limiting emission measure for detection is lower than this value.

4. Photometric calibration

A photometric calibration is performed by comparing the counts per second in the integrated profile of an HII region with its flux measured photoelectrically by Caplan and Deharveng (private communication ; herafter CD); their fluxes are obtained in the same way as the Hα and Hβ fluxes obtained for HII regions in the Large Magellanic Cloud (Caplan & Deharveng 1985). For each field we find a linear relation between CD's Hα fluxes and the measured counts in the present work. We have repeated this procedure for each observed field which has some common HII regions. From these we estimate a conversion factor: 1 ph/s equivalent to an Hα flux of about 4 10^{-12}erg.cm^{-2}s^{-1} (accurate within a factor of 2). For some fields there are no HII regions in common with CD; however, since there is a significant overlap between observed fields, we can select a previously calibrated HII region in the adjacent field. The Hα fluxes we obtain can be compared with those of other authors (Kennicutt & Hodge (1986), Copetti & Dottori (1989).

Kennicutt & Hodge (1986) obtained photographic Hα fluxes of 99 DEM regions. They have calibrated their Schmidt plates by means of independent photoelectric photometry of some HII regions appearing in the plates. The sampling angular resolution is comparable or worse to that of the present work. We have 32 regions in common but all of them at larger diaphragm sizes. On several ocasions their aperture encloses several HII regions. In order to make a comparison with their data, we have computed the Hα fluxes of 16 common regions using the same diaphragm as that of Kennicutt & Hodge (1986). The obtained fluxes agree with these authors although for faint HII regions our results are more accurate because our fluxes are photoelectric and this ensures high linearity even for weak emission. More recent work of Copetti & Dottori (1989) gives photoelectric Hβ fluxes of 30 DEM regions. We have 15 regions in common but again, the fluxes were measured with different apertures than ours. Nevertheless, we estimate a Hα/Hβ flux ratio of 3.69 ± 1.78 from their Hβ measures and the Hα fluxes presented in this work. Although highly uncertain, because no correction has been applied for the different diaphragm sizes, this line-ratio is in agreement with the average value derived from spectrophotometric observations (Peimbert & Torres-Peimbert 1976).

5. Results

5.1. Velocity field

Once the interferograms are flat-field corrected and the night-sky lines are subtracted, one can determine the velocity profile for each pixel in the field. For each profile obtained in this way we can determine a mean velocity by taking the barycenter of the profile distribution. This works quite well when the profile has a single component, however it would give a confused result when the profile has several velocity components. For a general view of the velocity field we have plotted it in a colour representation (Fig 3). At first glance, the SMC seems to behave as a rotating bar. Some discussion on this field is given in Sect. 6.

5.2. Diffuse ionized hydrogen

Figure 2 shows the image of the SMC given by mosaicing the monochromatic maps of 20 elementary fields. Each field has been exposed 2 hours. Similar maps can be constructed for each velocity channel. In Fig. 2 we have not included the fields corresponding to the Eastern zone of the SMC where the superbubble SMC1 (Meaburn 1980) is found. This will be studied in another work.

As each field contains some HII regions which have been measured photoelectrically by CD and the overlap between adjacent fields photometric continuity is ensures over over all of SMC (see Sect. 4). The image shown in Fig. 2 has a detection limit 5 times better than the limiting flux of the photographic atlas of Davies et al. (1976). Thus we detect almost all the DEM regions as well as several fainter structures and diffuse ionized hydrogen which are appreciated better in those regions not contaminated by the emission of DEM nebulae. The existence of the diffuse ionized hydrogen has been already detected by Torres & Carranza (1987). These structures are well correlated with those seen in IRAS images at 60 microns, which can be explained by a heating process by the UV emission. The very diffuse emission detected over the whole SMC shows, in its kinematics, a multi-component broad line structure. An example of this emission is given in Fig. 1. The whole galactic distribution of the diffuse ionized hydrogen, its flux and its kinematic structure will be discussed elsewhere.

5.3. HII region catalogue

Davies et al. (1976) have catalogued 167 regions of the SMC detected in Schmidt plates through an Hα+[NII] filter. They give the equatorial coordinates, the angular diameter and an estimate of the nebular brightnes.

Here we present the catalogue of radial velocities and fluxes of the DEM regions in the SMC. Not included in this catalogue are:

- The superbubble SMC1 located at the East of the K1 region and the giant complex N66 (DEM103) which will be the subject of other work.
- The first six regions of the DEM catalogue which are located at the Western boundary of our coverage.
- Some regions which, even if they have a DEM number, do not appear in the DEM charts.
- Some DEM regions which have been revealed to be galaxies or clusters.
- Several very faint regions either knots or diffuse and large diameter nebulæ.

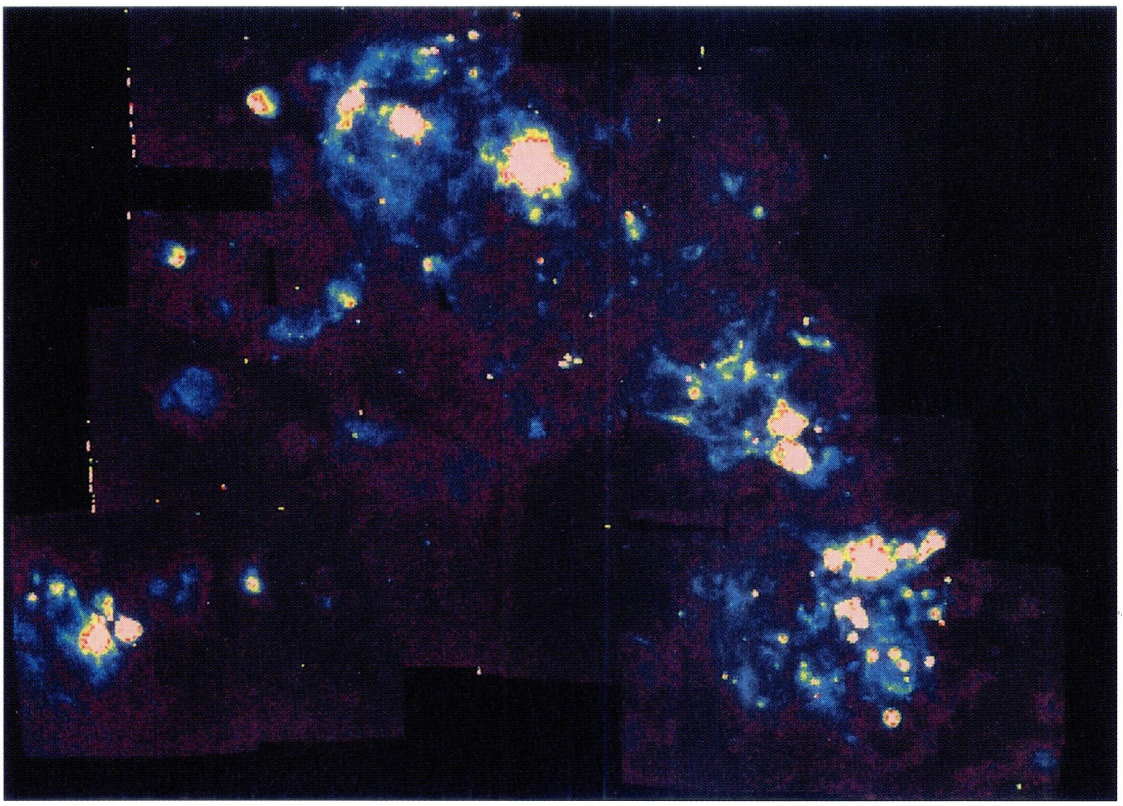

Fig. 2. Monochromatic map of the SMC in the Hα line. The intensities are coded with a rainbow lookup table

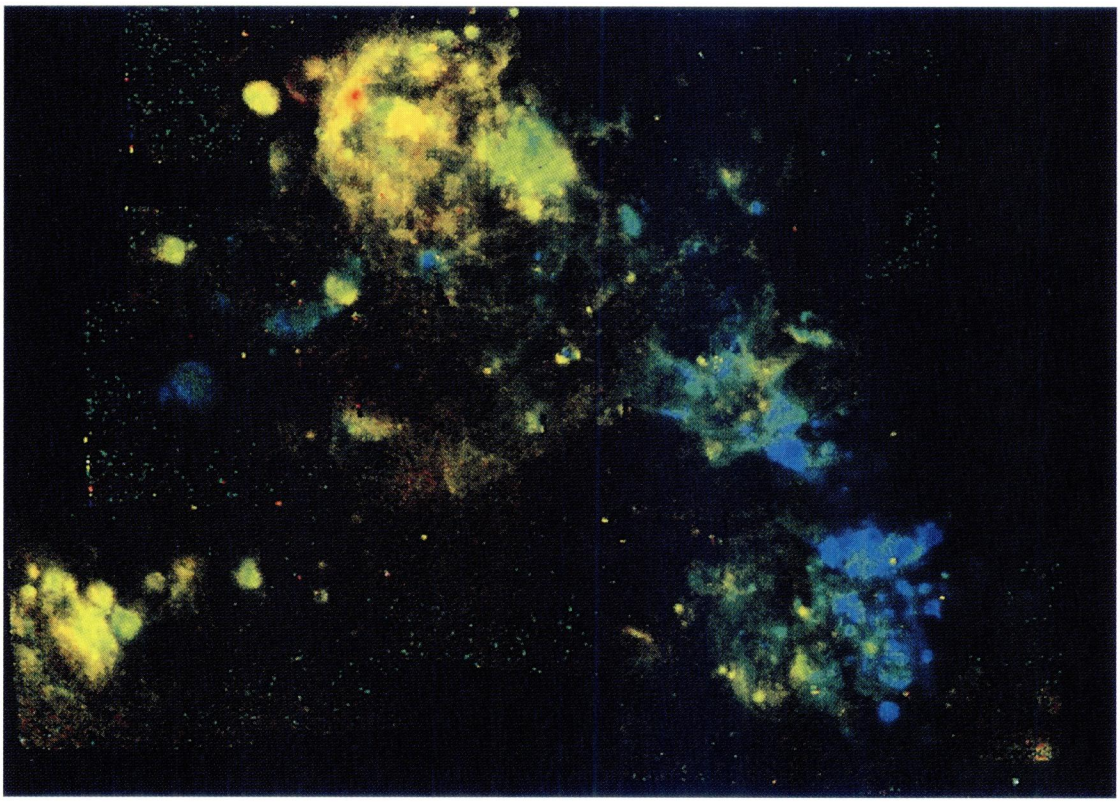

Fig. 3. Velocity field of the SMC, the color gives an idea of the value of the velocity, and the HII brightness is shown by the intensity of the color. Dark blue= 110 kms^{-1}, light blue=140kms^{-1}, green=155kms^{-1}, yellow=170 kms^{-1}, red=190kms^{-1} and white=205kms^{-1}

Thus we studied 143 regions from a total of 167 catalogued by DEM. We obtain integrated velocity profiles of each studied nebula over a small region centered on the brightest part of the nebula. The velocity profile is a convolution of the instrumental function (already discussed in Sect. 2), obtained from the Ne calibrations at 659.895 nm wavelength, and a Gaussian representing the Hα emission of the nebula whose width is broadened by thermal and internal motions. The night-sky lines mentioned in Sect. 3 are clearly distinguished and subtracted. Given the free-spectral range of the interferometer used in this work, the continuum level is easily established. The calibration in velocity is performed by means of the calibration interferograms taken with a hydrogen lamp (Sect. 2). The velocity accuracy in these determinations is about 2 kms^{-1}. Some fields were calibrated with the Ne calibration interferograms. In those cases, we have corrected for the phase variation due to the larger wavelength of the calibration; nevertheless, the radial velocities are accurate only in about 5 kms^{-1} for these cases. In very few cases the observed profile shows splittings. This could be due to several reasons: several different regions seen in the same direction, violent internal motions of a single nebula, traces of the complex structure of the HI in that region, etc. In those cases we were able to fit several Gaussians to the observed profile. The normal procedure of profile decomposition is:

– To obtain, from the nebular interferograms (once corrected for flat-field) and the phase-map, the profile of the selected area.

– To obtain, from the Ne calibration interferograms, the instrumental function of the same selected area.

– To identify the night-sky lines and subtract them, if necessary.

– To perform a convolution of a proposed Gaussian with the instrumental function already known. The result of this convolution is visually matched to the observed profile. By trial and error we finally propose the Gaussian which most closely simulates (once convoluted with the Airy function) the observed profile. The width of this Gaussian is taken as the velocity dispersion of the HII region. When the profiles are complex, the specialized software is capable of deconvolving several proposed Gaussians, co-adding them and giving the final result superposed on the original profile.

In this way we obtain the radial velocities of one or several components of the any region. The computed widths of the Gaussians give the velocity dispersion, σ, of that velocity component corrected for the instrumental function. The use of a Ne lamp instead of an H lamp for this purpose introduces an additional broadenning due to the fine structure of the Hα of 6.5 kms^{-1} which must be taken into account. On the other hand, in order to interpret the velocity dispersions as true internal motions in the HII region, u, we must correct for thermal broadening, b. The classical way is to say that this latter effect can be subtracted from the Gaussian width in the following way:

$$\sigma^2 = u^2 + b^2$$

We have quoted the 'observed' value (already corrected for the instrumental function) instead of the true one because this latter value implies a knowledge of the gas temperature. The Hα fluxes are calculated for each velocity component following the

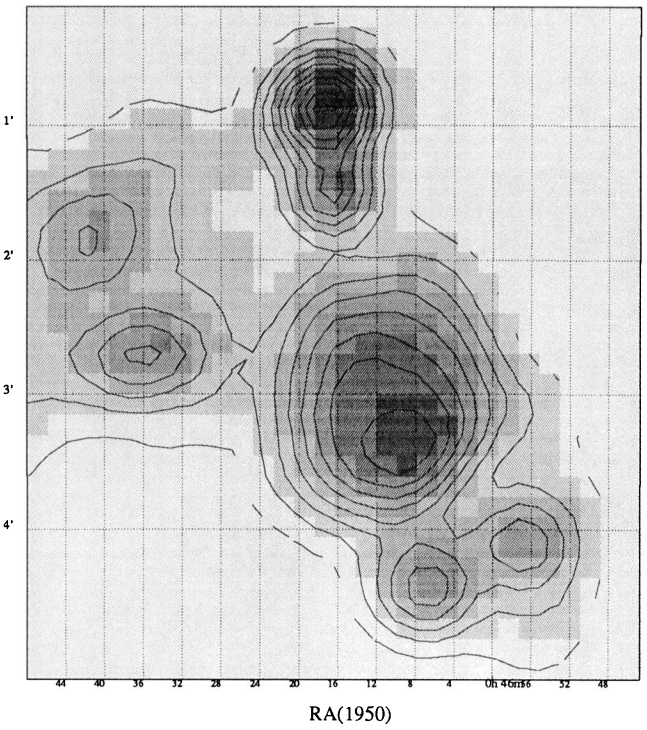

Fig. 4. Monochromatic image of the region of DEM 43 in the Hα line

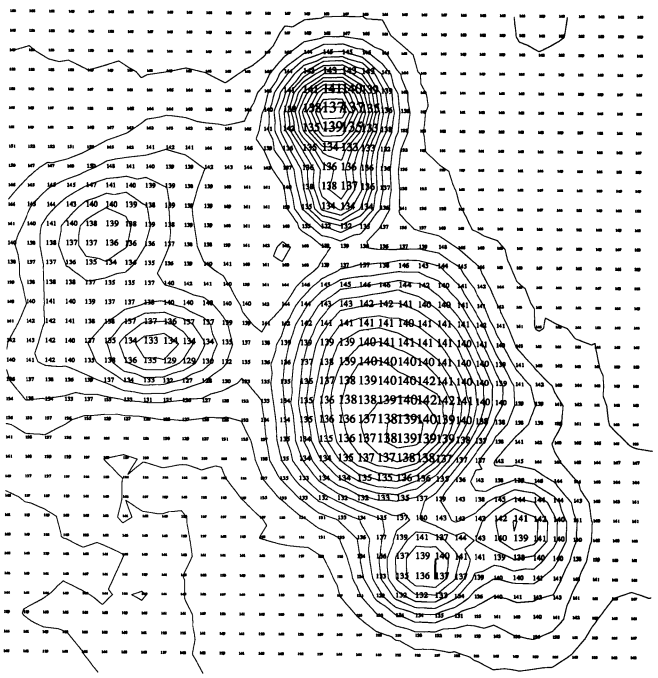

Fig. 5. Radial velocity field superposed to a contour plot representation of the monochromatic image of the same region

discussion given in Sect. 4, after finding the conversion factor for the selected frame. In this way, we have completed the HII region catalogue of Davies et al. (1976), with an estimation of the radial velocity, the velocity dispersion, the flux at Hα and a spectral decomposition. for example the association DEM 35,37,38,43 was mapped in this way. Figure 4 shows a monochromatic image of this region; in Figure 5 the whole velocity map is shown written on an isophote contour plot of the nebulae, and Figure 6 gives a representation of these velocities over the same plot.

Table 1 (accessible in electronic form) is the catalogue. In it, the first column gives the number of the nebula in the DEM catalogue; columns 2 and 3 give the equatorial coordinates of the center of the nebula referred to 1950; column 4 gives the heliocentric radial velocity of the nebular components in kms^{-1}; column 5 gives the velocity dispersion in kms^{-1}, corrected only for the instrumental function as discussed above; column 6 gives the size of the area over which the integrated profile was obtained for the flux determination, in arcmin; column 7 gives the Hα flux of each component in units of 10^{-10}ergs $cm^{-2}s^{-1}$ and column 8 gives the comments, used mainly when the velocity profile shows complex structure.

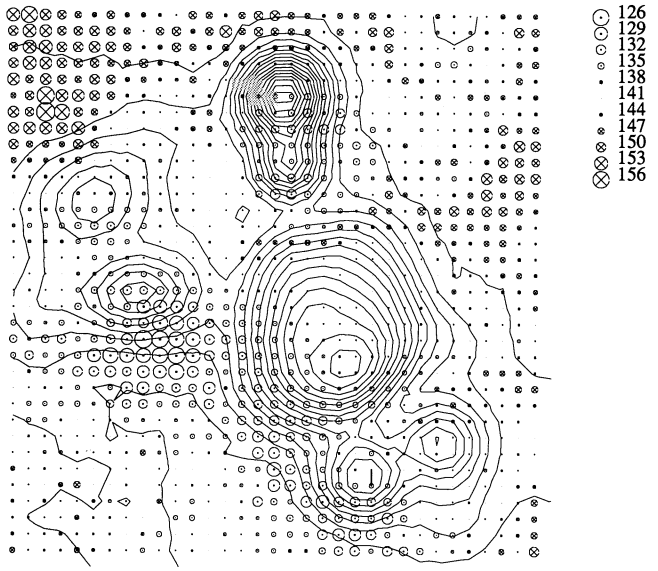

Fig. 6. Representation of the point radial velocities relative to the mean velocity: . approaching velocities, × receding velocities

6. Comparison with other kinematical data

6.1. Ionized hydrogen velocities

We have compared the kinematical data quoted in the catalogue with the data of other observers. The main sources of radial velocity data of SMC nebulæ are those of Smith & Weedman (1973) and Feast (1970). Smith & Weedman (1973) give the radial velocities and velocity dispersions of 30 SMC HII regions. They obtained the data by using a pressure scanned FP interferometer having a spectral resolution of 11 km/s, attached to a photometer, using the [OIII] line at lambda 500.7 nm. They obtain integrated profiles over the area covered by the diaphragm, mainly 3′ for almost all the regions studied. They obtain also the velocity dispersion of each region. We have 18 regions in common with which we can compare our radial velocities and velocity dispersions. In the case of the radial velocities there is a good correlation between our data and those of Smith & Weedman (1973), finding:

$$V_{r(\text{this survey})} = (6.69 \pm 6.18) + (0.95 \pm 0.04) V_{r(\text{SW})}$$

Indicating the same slope but an imprecision in the zero-point of the velocities of about 6 kms^{-1}. This could be due to several causes: differences in the area covered by the diaphragms, the calibration of the [OIII] velocities through Hα velocities of some HII regions, etc.

On the contrary, velocity dispersions are quite different. The values from the present work are larger, roughly by a factor of two, than those reported by Smith & Weedman (1973). Thermal broadening cannot be invoked in a simple way to explain this difference, in the Hα and [OIII] velocity dispersions because, in general, these emissions do not share the same volume. Thus, no direct comparison can be made between velocity dispersions at Hα and [OIII] and consequently, we cannot obtain the temperature of the emitting gas. We have thus observed some of our

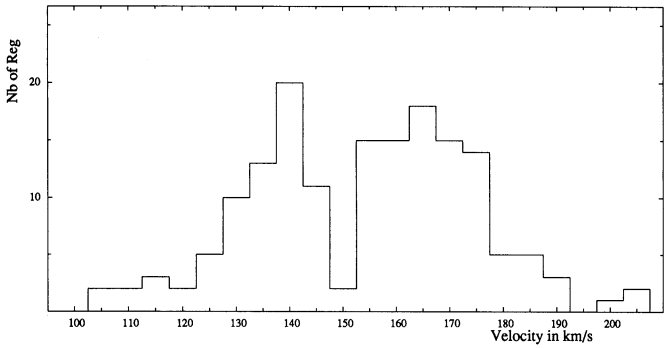

Fig. 7. Histogram of the velocities of the SMC HII regions of the catalogue reported in this work

frames also in [OIII]($\lambda\lambda$ 5007) and we obtain a rough agreement with Smith & Weedman's (1973) velocity dispersions of common HII regions. In the case of Feast (1970) data, this author studies 15 nebulæ with a Coudé spectrograph reporting standard errors between 2.8 to 7 kms^{-1}. We have only 7 common regions. A fit between our data and Feast's data gives:

$$V_{r\text{survey}} = (6.29 \pm 14.44) + (0.96 \pm 0.1) V_{r\text{Feast}}$$

Again, the slope is the same but the zero point velocity seems to be highly inaccurate, reflecting inaccuracies in both set of data.

6.2. HI velocities

From the more sensitive HI surveys of the SMC (Bajaja & Loiseau 1982 and Mc Gee & Newton 1981), we have used the data of Mc Gee & Newton (1981) in order to compare the obtained data with those of HI. The HI data of Mc Gee & Newton (1981) have an angular resolution of 15′, a spectral resolution of 8.2 kms^{-1} and the data are given for a mesh of about 7′ ×

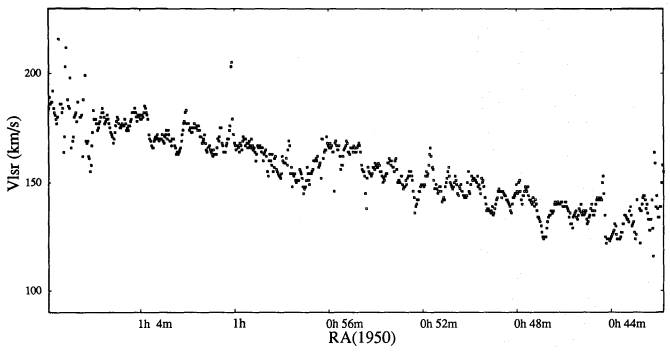

Fig. 8. Cut along the SMC bar 10 pixels wide showing the gradient of velocity along the bar

7′ . These authors give, in a microfiche form, the velocity profiles. We have printed and amplified these profiles and we have estimated, 'by inspection', the velocities of the profile maxima. In almost all cases the separation in different velocity components, by means of this procedure, is easy to do, however, in some cases the velocity profile is so complex that no attempt of decomposition by inspection has been made. On the other hand, we have based our positions on the coordinates reported by each profile. In several cases the coordinates of the region fall intermediate between two mesh points each having different profiles thus, introducing an additional source of uncertainty. In any case we have compared the velocities of 117 catalogued HII regions with the velocities of the HI gas nearly at that position. We find, in general, a good correspondence between the HII region velocities and those of the HI peaks. Furthermore, in most of the cases when two or more peaks appear in the HI velocity profile, the HII region velocity is similar to that of the main peak. In other cases where we have reported composite profiles, the velocities of the components fit those of the composite peaks in HI profiles, while in other cases, the HI profile is single, fitting only one of the HII components, or vice versa. Thus, in general, the HII region distribution shows agreement with the HI velocity components.

We can try to correlate the velocities of the HII regions with those of the HI at the same position. For 117 points we find a shallow fit:

$$Vr_{\mathrm{HIIregion}} = (17.77 \pm 4.33) + (0.89 \pm 0.03) Vrs_{\mathrm{HI}}$$

The different slope and the large disagreement of the zero-points is due to the inclusion of some nebulæ whose radial velocities deviate very much from those of the HI, while most of the nebulæ have velocities in good agreement with the HI gas. In fact, from 117 velocity points, 90 deviate by less than 8 kms^{-1} between the HII region and HI radial velocities.

7. Discussion

Figure 7 shows a histogram of the velocities of the SMC HII regions of the catalogue reported in this work. In this figure each velocity box corresponds to 5 km/s which is the highest velocity inaccuracy of the radial velocity data. One can see two main peaks at about 140 km/s and 170 kms/s and two secondary peaks at about 110 and 200 kms/s. This correspond to the four velocity components found by Martin et al. (1989) from a measurement of star velocities and a reinterpretation of the HI data of Mc Gee & Newton (1981). These components (L, H, VL and VH respectively) are assumed to be large complexes of gas and stars located at different depth along the line of view. Figure 8 is a cut along the SMC bar 10 pixels wide. This figure shows the gradient of velocity along the bar already found by Hindman (1967). A complete study of the kinematical properties of this galaxy, based on the HII regions and diffuse H^+ would be very interesting.

From the above results and discussion we arrive at the following conclusions:

–We have obtained kinematic observations of the HII regions and ionized hydrogen in the SMC. These observations are of high sensitivity and their accuracy has been tested by comparison with data obtained by other authors . This allows us to make a kinematical catalogue of HII regions in the SMC.

–While SMC HII regions show only one velocity component, the velocity profiles of the diffuse H^+ are broad and they indicate the presence of several velocity components as in the case of the HI.

–The HII region distribution follows the trend of the HI velocity components. Thus, they can be used as tracers of the young population in the SMC.

Acknowledgements. The authors wish to thank Philippe Amram, Jacques Boulesteix, Marie France Duval, Yvonne Georgelin, Annie Laval, Michel Marcelin, Patrice Joulie and Jean Urios who do this project feasible. They acknowledge financial founds and facilities from the INSU and ESO in the development of the instrument and the availability of an observing site. They gratful to Lise Deharveng and Jim Caplan for kindly allowing them to use their Halpha fluxes of several HII regions in the SMC, to James Lequeux for his encouragement to continue this work. To Annie Laval and Paris Pismis for the interesting comments they made when reading the manuscript. This work was also partially supported by a postdoctoral fellowship of the Commission of the European Communities and of DGAPA-UNAM and by the DGAPA grant IN102092.

References

Amram,P., Boulesteix, J., Georgelin, Y.P. et al.: The Messenger **64**, 44
Bajaja, E., Loiseau, N. (1982): A&AS **48**, 71
Caplan, J., Deharveng, L. (CD), (1993): Priv. Comm.
Caplan, J., Deharveng, L. (1985): A&AS **62**, 63
Copetti, M.V.F., Dottori, H.A. (1989): A&AS **77**, 327
Davies, R.D., Elliott, K.H., Meaburn, J., (DEM),(1976): MNRAS **81** 89
Dyson, J.E., Meaburn, J. 1971: A&A **12**, 219
Feast, M.W. 1970: MNRAS **149**, 291
Hindman, J.V. 1967: Aust. J. Phys. **20**, 147
Kennicutt, R.C., Hodge, P.W. 1986: ApJ **306**, 130
Laval, A., Rosado, M., Boulesteix, J. et al. 1989: A&A **208**, 230
Laval, A., Rosado, M., Boulesteix, J. et al. 1992: A&A **253**, 213
Le Coarer, E., Amram,P., Boulesteix, J. et al. 1992: A&A **257**, 389

Le Coarer, E., Rosado, M., Georgelin, Y.P. 1993: In: " New Aspects of Magellanic Cloud Research"- Lecture Notes in Physics. Eds. B. Baschek, G. Klare, J. Lequeux. Springer-Verlag. In press.
Martin, N., Maurice, E., Lequeux, J. 1989: A&A **215**, 219
Mc Gee, R.X., Newton, L.M. 1981: Proc. Astron. Soc. Australia **4**, 189
Meaburn, J. 1970: Nature **228**, 44.
Meaburn, J. 1980: MNRAS **192**, 365
Meaburn, J., Terrett, D.L., Mc Gee, R.X., Newton, L.M. 1984: MNRAS **206**, 705
Murai, T., Fujimoto, M. 1980: PAS Japan **32**, 581
Peimbert, M., Torres-Peimbert, S. 1976: ApJ **203**, 581
Rosado, M., Laval, A., Boulesteix, J. et al. 1990: A&A **238**, 315
Rosado, M., Laval, A., Le Coarer, E. et al. 1993: A&A, in press.
Smith, M.G., Weedman, D.W. 1973: ApJ **179** 461
Songaila, A., Blades, J.C., Hu, E.M., Cowie, L.L. 1986: ApJ **303**, 198
Torres, G., Carranza, G.J. 1987: MNRAS **226**, 513

This article was processed by the author using Springer-Verlag LaTeX A&A style file version 3.